Journal of Physics B: Atomic, Molecular and Optical Physics

Argon $1s^{-2}$ Auger hypersatellites

OPEN ACCESS
IOP Publishing
Journal of Physics B: Atomic, Molecular and Optical Physics
J. Phys. B: At. Mol. Opt. Phys. **54** (2021) 024001 (7pp)
https://doi.org/10.1088/1361-6455/abcd23

Argon $1s^{-2}$ Auger hypersatellites

Ralph Püttner[1,*], Yongjun Li[2], Jiaolong Zeng[2,3], Dimitris Koulentianos[4,5,9], Tatiana Marchenko[5,6], Renaud Guillemin[5,6], Loïc Journel[5,6], Oksana Travnikova[5,6], Moustafa Zmerli[5], Denis Céolin[6], Yoshiro Azuma[7], Satoshi Kosugi[7], Maria Novella Piancastelli[5,8] and Marc Simon[5,6]

[1] Institut für Experimentalphysik, Freie Universität Berlin, Arnimallee 14, D-14195 Berlin, Germany
[2] College of Liberal Arts and Science, National University of Defense Technology, Changsha, Hunan, 410073, People's Republic of China
[3] College of Science, Zhejiang University of Technology, Hangzhou Zhejiang 310023, People's Republic of China
[4] Department of Physics, University of Gothenburg, Origovägen 6B, SE-412 96 Gothenburg, Sweden
[5] Sorbonne Université, CNRS, Laboratoire de Chimie Physique-Matière et Rayonnement, LCPMR, F-75005 Paris Cedex 05, France
[6] Synchrotron Soleil, l'Orme des Merisiers, Saint-Aubin, F-91192 Gif-sur-Yvette Cedex, France
[7] Department of Materials and Life Sciences, Sophia University, Tokyo 102-8554, Japan
[8] Department of Physics and Astronomy, Uppsala University, SE-75120 Uppsala, Sweden

E-mail: puettner@physik.fu-berlin.de

Received 31 July 2020, revised 30 October 2020
Accepted for publication 23 November 2020
Published 30 December 2020

Abstract

The $1s^{-2}$ Auger hypersatellite spectrum of argon is studied experimentally and theoretically. In total, three transitions to the final states $1s^{-1}2p^{-2}(^2S^e,^2D^e)$ and $1s^{-1}2s^{-1}(^1S)2p^{-1}(^2P^o)$ are experimentally observed. The lifetime broadening of the $1s^{-2} \rightarrow 1s^{-1}2p^{-2}(^2S^e,^2D^e)$ states is determined to be 2.1(4) eV. For the used photon energy of $h\nu = 7500$ eV a KK/K ionisation ratio of $2.5(3) \times 10^{-4}$ is derived. Generally, a good agreement between the experimental and present theoretical energy positions, linewidths, and intensities is obtained.

Keywords: double core hole, Auger spectroscopy, HAXPES

(Some figures may appear in colour only in the online journal)

1. Introduction

Double core-hole (DCH) states are of high interest since they are more sensitive to chemical effects and electronic many-body effects than single core-hole (SCH) states [1, 2]. Already in the 1970s DCH states have been proven to exist by their radiative decay emitting an x-ray photon, see e.g. [3–5]. The corresponding x-ray photon energies are, however, not very sensitive to the individual core-hole states. Because of this, the investigation of DCH states based on the detection of the emitted electrons was a significant step forward. The pioneering works on this field are by Eland *et al* [6] and Lablanquie *et al* [7], who observed DCH states at synchrotron radiation facilities using magnetic bottle detection as well as by Berrah *et al* [8], who used a free electron laser as a light source. These approaches provided access to K^{-2} DCH states of second-row elements via electron emission. Recently, part of the present authors showed that DCH states can be observed as shake-up states in single-channel photoemission, giving rise to the opportunity to observe $K^{-1}L^{-1}V$ (Ar, HCl) [9, 10] and even $K^{-2}V$ (SF_6, CS_2) DCH states [11] of third-row elements with binding energies between 3 and 5.2 keV; here V indicates the occupation of a normally unoccupied valence or Rydberg orbital.

Hypersatellites are the decay processes of such DCH states. Generally, these decay processes can be radiative

* Author to whom any correspondence should be addressed.
[9] Present address: Chemical Sciences and Engineering Division, Argonne National Laboratory, 9700 S Cass Avenue, Lemont, IL 60439, USA.

leading to x-ray hypersatellites or non-radiative causing Auger hypersatellites. As mentioned above, x-ray hypersatellites have been investigated since several decades, see e.g. references [3–5, 12, 13]. The fast development of synchrotron radiation sources and electron spectrometers for the hard x-ray regime made it possible to observe also the non-radiative Auger hypersatellites. In the year 2000 Pelicon and co-workers observed the most intense *KK*–*KLL* hypersatellite in neon [14]. Some years later Southworth *et al* [15] observed several Ne hypersatellites lines and derived from these data a value for the K/KK ionisation ratio. In 2016 this spectrum was remeasured with significantly improved statistics and resolution [16]. This allowed to assign the spectral features based on the observed linewidths and lineshapes to different processes like the decay of K^{-2} or $K^{-2}V$ states. Because of its relative simplicity the neon hypersatellite Auger spectrum was studied by several groups [14, 15, 17–20]. Very recently, the K^{-2} Auger hypersatellites of H_2O were reported giving indications for ultrafast molecular dynamics [21].

The DCH states of argon were also studied extensively in recent years, both experimentally and theoretically. Chen calculated the K^{-2} hypersatellite Auger spectrum as well as the core-hole lifetimes [18], while Dyall [22] calculated the population probability for the creation of *KK* and *KL* double core holes as a shake satellite of the Ar $1s^{-1}$ photoionisation. Moreover, Karim *et al* [23] calculated the radiative and non-radiative decay of hollow argon atoms. Experimentally, Mikkola and Ahopelto [24] studied the radiative $K\alpha^h$ hypersatellite spectrum of K^{-2} DCH state and Raboud *et al* [25] the x-ray hypersatellite spectrum of the *KL* mixed DCH spectrum. Finally, Püttner *et al* [9] measured the Ar $K^{-1}L^{-1}V$ shake-up photoelectron lines while Carniato [26] studied the Ar $K^{-2}V$ satellites theoretically. Here we present the spectrum of the K^{-2} Auger hypersatellites of Ar together with complementary calculations revealing for energy positions, linewidths, and intensities good agreement between experiment and theory.

2. Experimental details

The experiments were performed at the GALAXIES beamline of the French national synchrotron radiation facility SOLEIL [27]. The used endstation dedicated to hard x-ray photoelectron spectroscopy (HAXPES) experiments is described in detail in reference [28]. In short, the lens system of the analyser is mounted parallel to the polarisation vector of photon beam. The presented Auger spectra were recorded using two photon energies, namely 3.9 keV and 7.5 keV. The spectrum measured at $h\nu = 3.9$ keV is taken below the Ar $1s^{-2}$ threshold and shows the background of the spectrum with the Auger hypersatellites measured at $h\nu = 7.5$ keV. The data acquisition for the spectrum at $h\nu = 3.9$ and $h\nu = 7.5$ keV took about 1 h and 12 h, respectively. For the electron analyser a slit width of 800 μm and a pass energy of 500 eV were used, resulting in an experimental resolution of $\cong$ 1.0 eV. To calibrated the kinetic-energy axis the Ar $1s^{-1} \rightarrow 2p^{-2}(^1D_2)$ normal Auger transition at $E_{\mathrm{kin}} = 2660.51$ eV [29] was used.

3. Method of calculations

The Auger decays were calculated in the framework of perturbation theory implemented by the distorted wave approximation and using the flexible atomic code developed by Gu [30]. Details of the theoretical method can be found in references [20, 31] and thus here we only provide a short outline. The radial orbital wave functions are obtained by solving the Dirac–Fock–Slater equation. The configuration state functions (CSF) of an atomic ion with N electrons are antisymmetric sums of the products of N one-electron Dirac spinors. The atomic state functions are given by mixing the CSF of the same symmetry. The mixing coefficients and the energy levels of an atomic ion are obtained from diagonalising the relativistic Hamiltonian. The continuum electron wave functions are obtained using the distorted-wave approximation. In the first-order perturbation theory, single Auger decay rate can be written as

$$\mathrm{A}_{if} = \frac{4}{k_f}|\langle\Psi_f^+|V|\Psi_i\rangle|^2 \tag{1}$$

where k_f is the momentum of the Auger electron, $V = \sum_{i<j}^{N} \frac{1}{r_{ij}}$ contains Coulomb interactions between electrons, $|\Psi_i\rangle$ is the autoionising state and $|\Psi_f^+\rangle$ is the final state of one higher ionisation stage plus a continuum electron

$$|\Psi_f^+\rangle = \sum_{\kappa}|\Psi_f, \kappa; J_{\mathrm{T}}M_{\mathrm{T}}\rangle \tag{2}$$

where κ is the relativistic angular quantum number of the continuum electron, J_{T} and M_{T} are the total angular momentum and the projection of the total angular momentum of the coupled final state, which must be equal to that of $|\Psi_i\rangle$. To obtain the lifetime width of the state $1s^{-2}\ {}^1S^o$, in addition to single Auger decay, the direct double Auger decay was also calculated according to the separation of knock-out and shake-off mechanisms [32, 33]:

$$\mathrm{A}^2_{\mathrm{KO}} = \sum_m \mathrm{A}^1_{im}\sigma_{mf}(\varepsilon_0) \tag{3}$$

and

$$\mathrm{A}^2_{\mathrm{SO}} = \sum_m \mathrm{A}^1_{im}|\langle\Psi_f^{2+}|\Psi_m\rangle|^2 \tag{4}$$

where A^1_{im} is the single Auger decay rate from level i to m and $\sigma_{mf}(\varepsilon_0)$ is the electron impact ionisation cross section from m to f.

4. Data analysis and results

Figure 1 shows part of the Ar *KLL* and *KLM* Auger spectra measured at $h\nu = 3900$ eV, i.e. well below the $1s^{-2}$ double ionization threshold so that the Auger hypersatellite transitions do not contribute. Their energy range is, however, indicated and shows that the displayed spectrum forms the background of Auger hypersatellite spectrum. Contributions of the Ar *KLL* Auger spectrum can be found in form of Ar $1s^{-1}3l^{-1}n'l' \rightarrow 2p^{-2}(^1D)$ shake-down Auger decays and in form of the $1s^{-1} \rightarrow 2p^{-2}(^3P_2)$ normal Auger transitoin, which

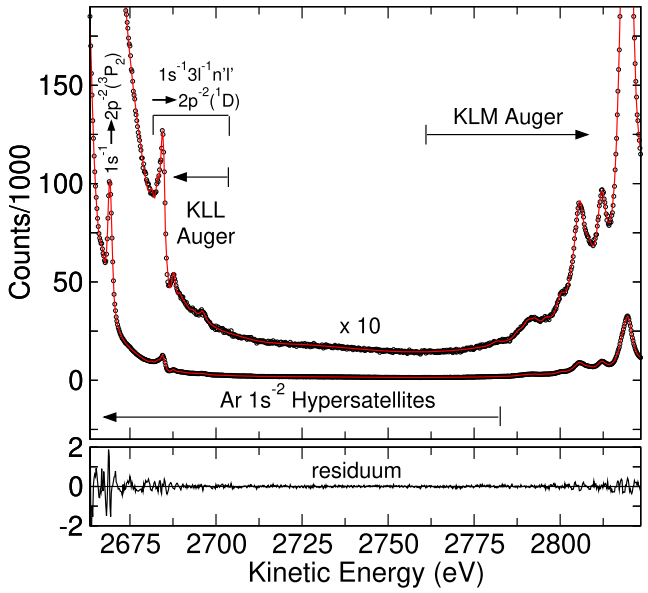

Figure 1. The argon Auger spectrum between 2663.38 and 2823.38 eV recorded at $h\nu = 3900$ eV. The red solid lines through the data points represent the fit result. The energy position of the $1s^{-1} \rightarrow 2p^{-2}(^3P_2)$ transition as well as the energy regions of the $1s^{-1}3l^{-1}n'l' \rightarrow 2p^{-2}(^1D_2)$ transitions (both part of the *KLL* Auger transitions), the *KLM* Auger transitions, and the Ar $1s^{-2}$ Auger hypersatellites are indicated. For more details, see text. For the residuum shown in the lower part the ordinate is stretched by a factor of 10 as compared to that of the spectrum.

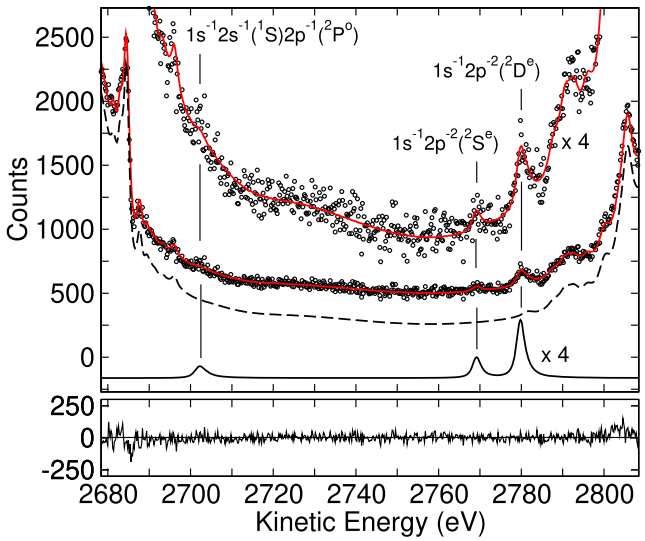

Figure 2. The argon Auger spectrum between 2678.38 and 2808.38 eV recorded at $h\nu = 7500$ eV. The red solid lines through the data points represent the fit result. The dashed and solid subspectra show the background obtained from the 3900 eV spectrum and the Ar $1s^{-2}$ hypersatellite contributions, respectively. The vertical lines serve as guide to the eye by relating the same features in the different spectra and connect them to their assignment. The lower part of the figure displays the residuum.

are present up to kinetic energies of ≅ 2700 eV [34] while those of the *KLM* Auger decay start at ≅ 2760 eV in form of Ar $1s^{-1} \rightarrow 2s^{-1}3s^{-1}3l^{-1}n'l'$ shake satellites of the Auger decay. Moreover, the background of the relevant part of the spectrum is also influenced by the shoulders of the Lorentzian lineshapes of the much more intense *KLL* and *KLM* diagram lines. Finally, the spectrum shows around 2730 eV a very weak and about 15 eV broad feature which could not be assigned in this work.

Since the Ar $1s^{-2}$ Auger hypersatellites possess low intensities compared to most of the background features, see above, an excellent knowledge about the background is required. For this purpose an Auger spectrum with good signal-to-noise-ratio was measured at a photon energy of $h\nu = 3900$ eV and shown in figure 1. The selected photon energy is well below the Ar $1s^{-2}$ double ionisation threshold at 6656.1(1.4) eV determined by $E_{\rm bin}(1s^{-2}) = E(K\alpha_2^h) + E_{\rm bin}(1s^{-1}2p^{-1}(^1P_1))$. Here, $E(K\alpha_2^h) = 3133.0(1.0)$ eV is the energy of the x-ray hypersatellite line for the $1s^{-2}(^1S_0) \rightarrow 1s^{-1}2p^{-1}(^1P_1)$ transition [24] and $E_{\rm bin}(1s^{-1}2p^{-1}(^1P_1)) = 3523.1(4)$ eV the binding energy for the Ar $1s^{-1}2p^{-1}(^1P_1)$ DCH state [9]. The obtained value agrees very well with the value of $E_{\rm bin}(1s^{-2}) = 6656.3(1.5)$ eV based on the $K\alpha_2^h$ hypersatellite line, a radiative *KL–LL* hypersatellite line, the Ar $1s^{-1}$ binding energy, and the $KL_{2,3}L_{2,3}(^1D_2)$ Auger line [24]. The present theoretical Ar $1s^{-2}$ double ionisation threshold is calculated to $E_{\rm bin,theo}(1s^{-2}) =$ 6653 eV, which also agrees very well with both experimental and the theoretical result of $E_{\rm bin,theo}(1s^{-2}) = 6654.1$ eV given in reference [24]

To simulate the background for the spectrum shown in figure 2, which was measured at $h\nu = 7500$ eV and reveals Ar $1s^{-2}$ Auger hypersatellites, the present spectrum was fitted using about 35 Lorentzian and Gaussian lines to describe the *KLL* and *KLM* Auger transitions; to simulate the experimental resolution all lines were convoluted with a Gaussian of 1 eV full width at half maximum (FWHM). The result of the fit is represented by the red solid line through the data points. The main aim of this fit approach was not to obtain lines with physical meaning, but to obtain in the region of the argon Auger hypersatellites a residuum without structures, as shown by the solid line in the lower part of figure 1.

In the next step the Auger spectrum recorded at $h\nu =$ 7500 eV including the Ar $1s^{-2}$ hypersatellites was fitted by using as background the fit result obtained for the spectrum at $h\nu = 3900$ eV. This background was adapted to the spectrum measured at $h\nu = 7500$ eV by using only two free parameters, namely a factor to account for a different count rates and an additional constant background. In addition to the features already described with the background, the spectrum contains three peaks of low intensity, which were attributed to Ar $1s^{-2}$ hypersatellites and assigned based on calculations. These features were fitted with post collision interaction (PCI) lineshapes since such asymmetric lineshapes were found for the $1s^{-2}$ hypersatellites of neon [16]. The origin of this PCI lineshape resides in the energy sharing of the electrons in double ionization process stimulated by one photon. In such double ionization processes the sharing can be described with a typical 'U-shape' of the kinetic-energy distribution [7], i.e. most likely one electron will be fast and the other one slow. As typical for PCI, the slow photoelectron screens in the subsequent decay process the ionic core and accelerates the fast Auger electron,

Table 1. Summary of the fit results of the Ar $1s^{-2}$ Auger transitions to the different final states. Given are the Auger energies E_{Auger}, the relative intensities, and the lifetime broadenings Γ. The numbers in parentheses indicate the error bars.

Final state	E_{Auger} (eV)		Intensity (arb. units)	Γ (eV)	
	Expt.	Theory		Expt.	Theory
$1s^{-1}2s^{-1}(^1S)2p^{-1}(^2P^o)$	2701.77(90)	2698.68	114(41)	3.0 (fixed)	4.001
$1s^{-1}2p^{-2}(^2S^e)$	2768.95(48)	2769.59	140(32)	2.1(4)	2.509
$1s^{-1}2p^{-2}(^2D^e)$	2779.60(36)	2779.20	394(44)	2.1(4)	2.551

Table 2. Theoretical Auger energies E_{Auger}, Auger rates, BRs, and lifetime broadenings Γ for the Auger decay channels of the Ar $1s^{-2}$. Given are the main channels with Auger rates larger than 2.0×10^{13} s^{-1}. The numbers in parentheses indicate the power of ten.

Group	Final state	E_{Auger} (eV)	Rate (s^{-1})	Γ (eV)	BR (%)
KK–KMM	$1s^{-1}3p^{-2}(^2D^e)$	3372.31	2.045(13)	2.145	0.99
KK–KLM	$1s^{-1}2p^{-1}(^3P)3p^{-1}(^2D^e)$	3091.60	5.916(13)	2.381	2.86
KK–KLM	$1s^{-1}2p^{-1}(^3P)3p^{-1}(^2P^e)$	3090.23	5.043(13)	2.317	2.43
KK–KLM	$1s^{-1}2p^{-1}(^1P)3p^{-1}(^2D^e)$	3082.42	1.248(14)	2.282	6.02
KK–KLM	$1s^{-1}2p^{-1}(^3P)3s^{-1}(^2P^o)$	3076.57	2.333(13)	2.293	1.13
KK–KLM	$1s^{-1}2s^{-1}(^3S)3p^{-1}(^2P^o)$	3021.51	2.272(13)	3.155	1.10
KK–KLM	$1s^{-1}2s^{-1}(^1S)3p^{-1}(^2P^o)$	3005.96	4.951(13)	3.677	2.39
KK–KLL	$1s^{-1}2p^{-2}(^2D^e)$	2779.20	9.012(14)	2.551	43.49
KK–KLL	$1s^{-1}2p^{-2}(^2P^e)$	2775.70	7.156(13)	2.505	3.45
KK–KLL	$1s^{-1}2p^{-2}(^2S^e)$	2769.59	9.402(13)	2.509	4.54
KK–KLL	$1s^{-1}2s^{-1}(^3S)2p^{-1}(^2P^o)$	2711.05	2.203(13)	2.575	1.06
KK–KLL	$1s^{-1}2s^{-1}(^1S)2p^{-1}(^2P^o)$	2698.68	3.899(14)	4.001	18.82
KK–KLL	$1s^{-1}2s^{-1}(^2S^e)$	2635.45	7.510(13)	2.743	3.62
	Sum minor decay channels		1.677(14)		8.09
All	All channels		2.072(15)		100.00

which in this way obtains the characteristic asymmetric line shape.

The PCI profiles are described by a Kuchiev and Sheinerman line shape [35], which is used in the present work in its simplified form given by Armen *et al* [36]. This formula contains the energy position of the Auger transition in absence of the PCI shift, therefore the actual energy positions in the spectrum are slightly higher. Note that such values are given in table 1. The PCI shift is calculated based on the natural linewidth Γ and the kinetic energy of the photoelectron, which is in the present case only an effective parameter since the energy sharing between the two photoelectrons is continuous. During the fit, the two Auger transitions to the final state configuration $1s^{-1}2p^{-2}$ were described with identical linewidths and effective parameters for the lineshape distortion, while for the Auger transition to the final state configuration $1s^{-1}2s^{-1}2p^{-1}$ different values were used. This is necessary since $2s^{-1}$ and $2p^{-1}$ core holes exhibit signicantly different linewidths. The obtained PCI lineshapes were convoluted with a Gaussian function of 1.0 eV FWHM in order to simulate the experimental resolution caused by the analyser.

The fit results for the $1s^{-2}$ Auger hypersatellites are presented by the solid subspectrum in figure 2 and summarised in table 1. The obtained $\chi^2 = 856$ is in the order of the data points (651 points) and shows, together with the residuum, the quality of the fit. The results shown in figure 2 clearly demonstrate the necessity of the elaborated background description since the $1s^{-2} \rightarrow 1s^{-1}2p^{-2}(^2D^e)$ Auger transition at ≅ 2780 eV overlaps with a *KLM* Auger transition to a $2s^{-1}3s^{-1}3l^{-1}n'l'$ final state at ≅ 2782 eV, both with comparable widths of more than 2 eV.

From the fit analysis the lifetime broadening for the Auger transitions to the $1s^{-1}2p^{-2}$ configuration resulted in Γ = 2.1(4) eV. As for all Ar $1s^{-2}$ Auger transitions the lifetime broadening consists of two contributions, namely the contribution of the Ar $1s^{-2}$ lifetime and the contribution of the lifetime of the individual final state. The present theoretical value for the lifetime width of the initial state $1s^{-2}(^1S^e)$ amounts to Γ = 1.602 eV, consisting of contributions from the single Auger width (Γ = 1.364 eV), the direct double Auger decay width (Γ = 0.032 eV) and the radiative width (Γ = 0.206 eV). The total width of 1.602 eV agrees quite well with the theoretical value of Γ = 1.684 eV obtained by Chen [18]. The calculated lifetime widths for the $1s^{-1}2p^{-2}(^2S^e)$ and the $1s^{-1}2p^{-2}$ $(^2D^e)$ states amount to Γ = 0.907 eV and 0.949 eV, respectively; both values consist of contributions from the single Auger width and the radiative width. With these values we obtain total widths of 2.509 eV for the $1s^{-2} \rightarrow 1s^{-1}2p^{-2}\,{}^2S^e$ transition and 2.551 eV for the $1s^{-2} \rightarrow 1s^{-1}2p^{-2}$ $^2D^e$ transition. Both values agree well with the fit result of Γ = 2.1(4) eV.

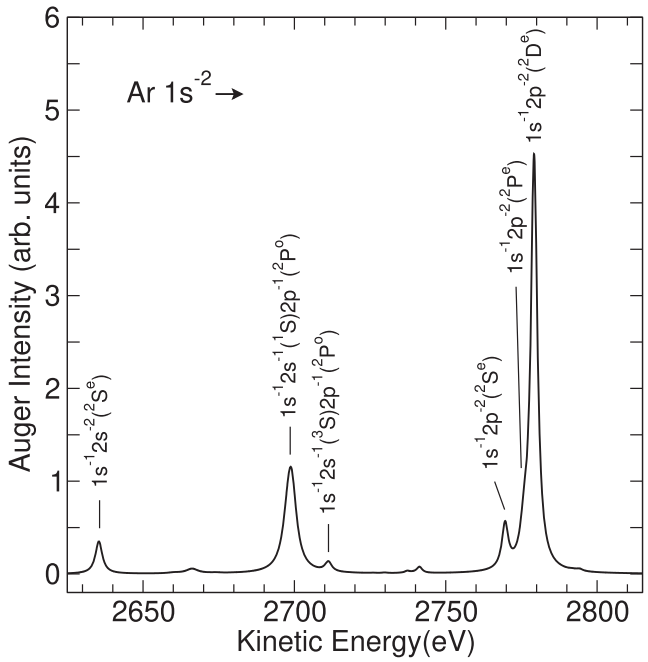

Figure 3. The calculated Auger spectrum of $Ar^{2+}1s^{-2}$ (^1S) in the electron energy range from 2625 to 2815 eV.

For the $1s^{-2} \rightarrow 1s^{-1}2s^{-1}(^1S)2p^{-1}(^2P^o)$ Auger transition the fit did not result in a physically meaningful value, due to insufficient signal-to-noise ratio; because of this the value was fixed to 3 eV. Theoretically the total width of this transition is calculated as 4.001 eV, with the lifetime width of the final state $1s^{-1}2s^{-1}(^1S)2p^{-1}$ ($^2P^o$) of 2.399 eV.

The calculated Auger energies, Auger rates, lifetime broadenings, and corresponding branching of the main Auger channels of the Ar $1s^{-2}$ DCH state are given in table 2. The theoretical spectrum of the Ar $1s^{-2}$ DCH state displaying the *KLL* Auger transitions in the energy range from 2625 to 2815 eV is shown in figure 3.

In the following we shall discuss the lifetime widths of the final states, which can readily be obtained from the widths given in table 2 by subtracting the Ar $1s^{-2}$ broadening of $\Gamma = 1.602$ eV. In a simple approach one may assume that this value can be obtained by the Ar $1s^{-1}$ core-hole lifetime and the Ar $2l^{-2}$ DCH lifetime. The latter values are given by $\Gamma(2s^{-2}) = 5.49(44)$ eV, $\Gamma(2s^{-1}2p^{-1}) = 2.17(2)$ eV [34] and $\Gamma(2p^{-2}) = 0.323(15)$ eV [38]. The partial Auger rate for the decay of the Ar $1s^{-1}$ core hole in the $1s^{-1}2p^{-2}$ configuration calculated by Bhalla [37] corresponds to a width of $\Gamma = 0.457$ eV. By taking this result as a typical value, one obtains for the sum of the width of the single core hole in the *K*-shell and the double core hole in the *L*-shell 0.780 eV for the $1s^{-1}2p^{-2}$ configuration. This value is in reasonable agreement with values between 0.903 to 0.949 eV obtained by the present calculations for this configuration. The same holds for the $1s^{-1}2s^{-1}(^1S)2p^{-1}$ ($^2P^o$) with a calculated value of 2.399 eV and a sum of 2.62 eV obtained from 2.17 eV for the $2s^{-1}2p^{-1}$ DCH-state and 0.45 eV for the $1s^{-1}$ SCH state. For other final states like $1s^{-1}2s^{-1}(^3S)2p^{-1}$ ($^2P^o$) and $1s^{-1}2s^{-2}$ ($^2S^e$) the calculated values are considerably smaller than the sums of the Ar $1s^{-1}$ SCH state and the $2l^{-2}$ DCH states. Obviously, the lifetime of triple core-hole states cannot simply be calculated by the sum of SCH and DCH states. This result is not surprising since already for DCH states it has been observed that the lifetime broadenings are not just the sum of the corresponding SCH states [9, 16, 38]. However, a detailed discussion of the lifetimes of triple core-hole states is beyond the scope of this study.

Finally we want to point out that the asymmetry in the lineshapes due to PCI is much less pronounced than in case of neon [16, 19]. We assume that this is due to the significantly higher excess energy $E_{exc} = h\nu - E_{bin}(1s^{-2}) \cong 850$ eV for Ar as compared to $E_{exc} = 435$ eV for Ne so that for a similar ratio for the energy sharing between the two electrons the slower electron for argon is expected to be faster by almost a factor of 2 as compared to neon.

As illustrated above, we used for the description of the Ar $1s^{-2}$ PCI lineshapes with the total widths of the peaks as lifetime broadening. It is discussed in reference [39] that this is only an approximation and a correct lineshape is given by a PCI lineshape using the Ar $1s^{-2}$ lifetime width convoluted with a Lorentzian lineshape defined by the lifetime of the Ar $1s^{-1}2(s,p)^{-2}$ Auger final state. Since such a convolution is not implemented in our fit program, we performed simulations for the final states of the $1s^{-1}2p^{-2}$ configuration. In this way we found for that configuration the following upper limits of the systematic errors: the obtained energy positions can be too large by up to 0.15 eV while the linewidths can be too small by up to 0.05 eV. Moreover, the convoluted lineshapes turned out to be slightly more symmetric, which may explain also partially the fact, that the lineshapes for argon in the present work are less asymmetric than those for neon [16, 19].

In the following we shall discuss the intensity ratios. The theoretical results in figure 3 show on the low-energy shoulder of the $1s^{-2} \rightarrow 1s^{-1}2p^{-2}(^2D^e)$ transition contributions of the weak $1s^{-2} \rightarrow 1s^{-1}2p^{-2}(^2P^e)$ transition, which we take into account in the following discussion. In this way we obtain a theoretical intensity ratio of 0.40 for $I(1s^{-2} \rightarrow 1s^{-1}2s^{-1}(^1S)2p^{-1}(^2P^o))$ divided by $I(1s^{-2} \rightarrow 1s^{-1}2p^{-2}(^2D^e))$ plus $I(1s^{-2} \rightarrow 1s^{-1}2p^{-2}(^2P^e))$ as well as 0.10 for $I(1s^{-2} \rightarrow 1s^{-1}2p^{-2}(^2S^e))$ divided by $I(1s^{-2} \rightarrow 1s^{-1}2p^{-2}(^2D^e))$ plus $I(1s^{-2} \rightarrow 1s^{-1}2p^{-2}(^2P^e))$, in perfect agreement with the calculations of Chen [18]. The experimental ratios are 0.29(15) and 0.36(13), respectively, i.e. for the $1s^{-2} \rightarrow 1s^{-1}2s^{-1}(^1S)2p^{-1}(^2P^o)$ transition they agree within the error bar. Although the difference for the $1s^{-2} \rightarrow 1s^{-1}2p^{-2}(^2S^e)$ transition is twice the error bar and, therefore, the statistical probability for such a deviation is in the order of 2%–3%, we consider this the most likely explanation. In principle, such an intensity effect can also be explained with different angular distributions of the Auger transitions, however, for pure inner-shell Auger processes the angular distribution is known to be rather isotropic.

From the present data we also derived the ratio KK/K, i.e. the Ar $1s^{-2}$ double to Ar $1s^{-1}$ single ionisation ratio, resulting in a value of $2.5(3) \times 10^{-4}$. To obtain this value we extracted from the present data the intensity ratio $I^{++}(^2D)/I^{+}(^3P_2) = 0.0135(2)$ of the most intense $1s^{-2} \rightarrow 1s^{-1}2p^{-2}(^2D)$ hypersatellite Auger transition to the $1s^{-1} \rightarrow 2p^{-2}(^3P_2)$

Auger transition, see figure 1. From the *KLL* Auger spectra presented in reference [34] we derived that the contribution of the $1s^{-1} \rightarrow 2p^{-2}(^3P_2)$ diagram line to the sum of all diagram lines is 1.00(5)%. This value agrees well with the experimental and theoretical values given by Krause of 1.0(2)% and 1.1%, respectively [40], however, with significantly improved error bars. For the Ar $1s^{-2}$ hypersatellites no experimental branching ratios (BRs) are available so that we use theoretical values. Here we would like to point out that on the low kinetic-energy side of the $1s^{-2} \rightarrow 1s^{-1}2p^{-2}(^2D)$ transition the $1s^{-2} \rightarrow 1s^{-1}2p^{-2}(^2P)$ transition may contribute as a shoulder to the measured intensity. The present theoretical branching ratio for the $1s^{-2} \rightarrow 1s^{-1}2p^{-2}(^2D)$ transition amounts to 0.4349 and the one for the $1s^{-2} \rightarrow 1s^{-1}2p^{-2}(^2P)$ transition 0.0345. Since it is unclear from the present fit analysis how the $1s^{-2} \rightarrow 1s^{-1}2p^{-2}(^2P)$ transition contribute to the obtained intensity of the peak assigned to the $1s^{-2} \rightarrow 1s^{-1}2p^{-2}(^2D)$ transition, we continue with the average value of 0.452(17); this value describes both possibilities, namely no contribution and full contribution of the $1s^{-2} \rightarrow 1s^{-1}2p^{-2}(^2P)$ transition, in terms of an average value and error bars. Note that the given BRs for the Ar $1s^{-2}$ double core hole include not only *KK*–*KLL* Auger decays, but also *KK*–*KLM* and *KK*–*KMM* Auger decays, see table 2. Contrary to this, for the branching ratio of 1.00(5)% for the $1s^{-1} \rightarrow 2p^{-2}(^3P_2)$ diagram line only the *KLL* transitions are taken into account. Because of this, the branching ratio has to be corrected to 0.87(4)% due to the BRs of $\cong 0.87 : 0.12 : 0.01$ for the *KLL* : *KLM* : *KMM* Auger decays of SCH creation of argon [29].

Finally we took into account BRs of the radiative decay for both the single and double *K*-shell vacancy, since radiative decay cannot be neglected. For the single *K*-shell vacancy an Auger branching ratio of 0.893(5) is found experimentally by Guillemin *et al* [41]. Contrary to this, for the double *K*-shell vacancy no experimental results are available so that we utilise two theoretical values, namely the present results of 0.852 and those of Chen [18] of 0.845, which we combine to a branching ratio of 0.848(4). In this way we result in the above given branching ratio for KK/K of $2.5(3) \times 10^{-4}$. This value agrees well with the value of 2×10^{-4} for the shake-off probability for the second Ar 1*s* electron after Ar $1s^{-1}$ core ionisation [22]. The present value is, however, significantly smaller than the experimental value of $7.5(8) \times 10^{-4}$ and theoretical value of 6.8×10^{-4} given for a photon energy of 23.3 keV [24]. This difference can probably be explained with contributions from knock-out processes, which are photon-energy dependent [33].

Note that in this estimation of the KK/K ratio the BRs of shake-up or double Auger processes are neglected. For single *K*-shell ionisation recent investigations show that the branching ratio for shake-up during the Auger amounts to 4.8(1.0)% [34] and the present calculations show for double *K*-shell ionisation that the branching ratio for the direct double Auger decay amounts to $\cong 2.3\%$ of the total Auger decays. These numbers justify neglecting these kinds of Auger decays.

5. Summary and perspectives

We presented a combined experimental and theoretical study of the Ar $1s^{-2}$ Auger hypersatellite decays. Experimentally, the three transitions to the final states $1s^{-1}2p^{-2}(^2S^e,^2D^e)$ and $1s^{-1}2s^{-1}(^1S)2p^{-1}(^2P^o)$ are observed. The two transitions Ar $1s^{-2} \rightarrow 1s^{-1}2p^{-2}(^2S^e,^2D^e)$ show an asymmetric lineshape due to PCI with a width of 2.1(4) eV, in good agreement with present theoretical values of $\cong 2.5$ eV. By comparing the experimentally observed intensities for argon Auger hypersatellites and *KLL* diagram lines for the photon energy of $h\nu = 7500$ eV the KK/K ionisation ratio was derived to $2.5(3) \times 10^{-4}$. Generally a good agreement between the experimental and the present theoretical energy positions, linewidths, and intensities was found.

We also tried to measure the Ar $K^{-2}V$ DCH states and their first-step Auger decay, however, contrary to neon without success due to the small cross section of these states [26]. In combination with the fact that DCH cross sections decrease with increasing atomic number *Z*, the present results on argon probably represent the current cutting edge of DCH investigations using electron detection due to available photon energies and photon fluxes.

Future improvements in flux and resolution at synchrotron facilities will allow investigating weak processes, such e.g. the creation of Ar $K^{-2}V$ states, elusive under the present conditions due to their low cross section.

Furthemore, with single-photon measurements it is not possible to study resonant Auger decay of states with a double core hole and one excited electron, because it is not possible to separate core ionization and core excitation.

The new high flux-short pulse x-ray free-electron laser sources will provide the ground for such studies, since it will be possible to induce core ionization with the absorption of a first photon and core excitation with the second photon.

In summary, the pioneering works on DCH electron spectroscopy, focusing on K^{-2} states of small molecules containing second-row elements [6–8], were recently extended to $K^{-1}L^{-1}$ and K^{-2} DCHs of atoms and molecules with the third-row elements [9–11]. The significantly higher photon energies available at the GALAXIES beamline after the planned upgrade will certainly allow to study DCH states of fourth-row atoms like V (e.g. $VOCl_3$), Ge ($GeCl_4$), Br (HBr), or Kr giving insight into deeper DCHs.

Acknowledgments

Experiments were performed on the GALAXIES beamline at SOLEIL Synchrotron, France (Proposal No. 99170136). We are grateful to SOLEIL staff for smoothly running the facility. DK wishes to acknowledge financial support from LabEx MiChem, France, as well as the Swedish Research Council (VR) and Knut and Alice Wallenberg Foundation, Sweden.

ORCID iDs

Ralph Püttner https://orcid.org/0000-0002-8761-6873
Tatiana Marchenko https://orcid.org/0000-0002-9015-3339
Loïc Journel https://orcid.org/0000-0001-8044-5437
Yoshiro Azuma https://orcid.org/0000-0001-8272-7868

References

[1] Cederbaum L S, Tarantelli F, Sgamellotti A and Schirmer J 1986 *J. Chem. Phys.* **85** 6513
[2] Santra R, Kryzhevoi N V and Cederbaum L S 2009 *Phys. Rev. Lett.* **103** 013002
[3] Ahopelto J, Rantavuori E and Keski-Rahkonen O 1972 *Phys. Scr.* **20** 71–4
[4] Richard P, Hodge W and Moore C F 1972 *Phys. Rev. Lett.* **29** 393
[5] Ågren H, Nordgren J, Selander L, Nordling C and Siegbahn K 1978 *J. Electron Spectrosc. Relat. Phenom.* **14** 27
[6] Eland J H D, Tashiro M, Linusson P, Ehara M, Ueda K and Feifel R 2010 *Phys. Rev. Lett.* **105** 213005
[7] Lablanquie P *et al* 2011 *Phys. Rev. Lett.* **106** 063003
[8] Berrah N *et al* 2011 *Proc. Natl Acad. Sci.* **108** 16912
[9] Püttner R *et al* 2015 *Phys. Rev. Lett.* **114** 093001
[10] Koulentianos D *et al* 2018 *Phys. Chem. Chem. Phys.* **20** 2724
[11] Feifel R *et al* 2017 *Sci. Rep.* **7** 13317
[12] Raju S S, Reddy B S, Murti M V R and Mombasawala L 2007 *X-Ray Spectrom.* **36** 35
[13] Soni S N 1999 *Indian J. Phys.* **73B** 661 http://hdl.handle.net/10821/5731
[14] Pelicon P, Čadež I, Žitnik M, Šmit Ž, Dolenc S, Mühleisen A and Hall R I 2000 *Phys. Rev.* A **62** 022704
[15] Southworth S H, Kanter E P, Krässig B, Young L, Armen G B, Levin J C, Ederer D L and Chen M H 2003 *Phys. Rev.* A **67** 062712
[16] Goldsztejn G *et al* 2016 *Phys. Rev. Lett.* **117** 133001
[17] Bhalla C P, Folland N O and Hein M A 1973 *Phys. Rev.* A **8** 649
[18] Chen M H 1991 *Phys. Rev.* A **44** 239
[19] Goldsztejn G *et al* 2017 *Phys. Rev.* A **96** 012513
[20] Li Y, Liu L, Gao C, Zeng J and Yuan J 2018 *J. Electron Spectrosc. Relat. Phenom.* **226** 26
[21] Marchenko T *et al* 2018 *Phys. Rev.* A **98** 063403
[22] Dyall K G 1983 *J. Phys. B: At. Mol. Phys.* **16** 3137
[23] Karim K R, Grabbe S R and Bhalla C P 1996 *J. Phys. B: At. Mol. Opt. Phys.* **29** 4007
[24] Mikkola E and Ahopelto J 1983 *Phys. Scr.* **27** 297
[25] Raboud P-A, Berset M, Dousse J-C, Maillard Y-P, Mauron O, Hoszowska J, Polasik M and Rzadkiewicz J 2002 *Phys. Rev.* A **65** 062503
[26] Carniato S 2020 *J. Electron Spectrosc. Relat. Phenom.* **239** 146931
[27] Rueff J-P *et al* 2015 *J. Synchrotron Radiat.* **22** 175
[28] Céolin D *et al* 2013 *J. Electron Spectrosc. Relat. Phenom.* **190** 188
[29] Asplund L, Kelfve P, Blomster B, Siegbahn H and Siegbahn K 1997 *Phys. Scr.* **16** 268–72
[30] Gu M F 2008 *Can. J. Phys.* **86** 675
[31] Zeng J L, Liu P F, Xiang W J and Yuan J M 2013 *Phys. Rev.* A **87** 033419
[32] Liu P, Zeng J and Yuan J 2018 *J. Phys. B: At. Mol. Opt. Phys.* **51** 075202
[33] Schneider T, Chocian P L and Rost J M 2002 *Phys. Rev. Lett.* **89** 073002
[34] Püttner R, Holzhey P, Hrast M, Žitnik M, Goldsztejn G, Marchenko T, Guillemin R, Journel L, Koulentianos D, Travnikova O, Zmerli M, Céolin D, Azuma Y, Kosugi S, Lago A F, Piancastelli M N and Simon M 2020 *Phys. Rev.* A **102** 052832
[35] Kuchiev M Y and Sheinerman S A 1986 *Zh. Eksp. Teor. Fiz.* **90** 1680
[36] Armen G B, Tulkki J, Aberg T and Crasemann B 1987 *Phys. Rev.* A **36** 5606
[37] Bhalla C P 1973 *Phys. Rev.* A **8** 2877
[38] Žitnik M *et al* 2016 *Phys. Rev.* A **93** 021401(R)
[39] Guillemin R *et al* 2015 *Phys. Rev.* A **92** 012503
[40] Krause M O 1975 *Phys. Rev. Lett.* **34** 633
[41] Guillemin R, Bomme C, Marin T, Journel L, Marchenko T, Kushawaha R K, Trcera N, Piancastelli M N and Simon M 2011 *Phys. Rev.* A **84** 063425